Chemical Science

ROYAL SOCIETY OF CHEMISTRY

EDGE ARTICLE

View Article Online
View Journal | View Issue

Cite this: *Chem. Sci.*, 2021, **12**, 2456

All publication charges for this article have been paid for by the Royal Society of Chemistry

Impact of sphingosine and acetylsphingosines on the aggregation and toxicity of metal-free and metal-treated amyloid-β†

Yelim Yi,[a] Yuxi Lin,‡[b] Jiyeon Han,‡[a] Hyuck Jin Lee,[c] Nahye Park,[d] Geewoo Nam,[d] Young S. Park,[d] Young-Ho Lee*[befg] and Mi Hee Lim*[a]

Pathophysiological shifts in the cerebral levels of sphingolipids in Alzheimer's disease (AD) patients suggest a link between sphingolipid metabolism and the disease pathology. Sphingosine (**SP**), a structural backbone of sphingolipids, is an amphiphilic molecule that is able to undergo aggregation into micelles and micellar aggregates. Considering its structural properties and cellular localization, we hypothesized that **SP** potentially interacts with amyloid-β (Aβ) and metal ions that are found as pathological components in AD-affected brains, with manifesting its reactivity towards metal-free Aβ and metal-bound Aβ (metal–Aβ). Herein, we report, *for the first time*, that **SP** is capable of interacting with both Aβ and metal ions and consequently affects the aggregation of metal-free Aβ and metal–Aβ. Moreover, incubation of **SP** with Aβ in the absence and presence of metal ions results in the aggravation of toxicity induced by metal-free Aβ and metal–Aβ in living cells. As the simplest acyl derivatives of **SP**, *N*-acetylsphingosine and 3-*O*-acetylsphingosine also influence metal-free Aβ and metal–Aβ aggregation to different degrees, compared to **SP**. Such slight structural modifications of **SP** neutralize its ability to exacerbate the cytotoxicity triggered by metal-free Aβ and metal–Aβ. Notably, the reactivity of **SP** and the acetylsphingosines towards metal-free Aβ and metal–Aβ is determined to be dependent on their formation of micelles and micellar aggregates. Our overall studies demonstrate that **SP** and its derivatives could directly interact with pathological factors in AD and modify their pathogenic properties at concentrations below and above critical aggregation concentrations.

Received 10th August 2020
Accepted 16th December 2020

DOI: 10.1039/d0sc04366d

rsc.li/chemical-science

Introduction

Accounting for approximately 50% of the brain's dry weight, lipids serve as signaling molecules, energy storage, and the building blocks of cellular membranes in neurons.[1,2] Sphingolipids, among the different types of lipids, are essential for the structural integrity of neuronal membranes with implications in cellular recognition, neurotransmission, myelin sheath formation, and apoptotic regulation.[3,4] Previous research has examined the pertinence of sphingolipid metabolism in brain homeostasis through the concept of sphingolipid rheostat, defined as the balance in the salvage pathway of sphingolipids.[5,6] For these reasons, multiple aspects of sphingolipids have been investigated with respect to the development, function, and homeostasis of the brain as well as neurodegeneration.[3,5,7–10]

As illustrated in Fig. 1a, sphingosine (**SP**) is an amino alcohol with an unsaturated hydrocarbon chain presenting the structural backbone of sphingolipids.[5,11,12] Amphiphilic compounds, including **SP**, are known to form micelles and micellar aggregates at concentrations above their critical aggregation concentrations (CACs).[13–17] Several reports suggest the subcellular localization of **SP** in the plasma membrane, cytosol, lysosome, mitochondria, Golgi apparatus, and endoplasmic reticulum.[7,18,19] As a component of cellular regulation circuits, **SP** is engaged in regulating the release of neurotransmitters by controlling pre-synaptic vesicle fusion under normal conditions.[20,21] In addition, pathological shifts in the sphingolipid rheostat manifesting increased levels of **SP** are associated with

[a]*Department of Chemistry, Korea Advanced Institute of Science and Technology (KAIST), Daejeon 34141, Republic of Korea. E-mail: miheelim@kaist.ac.kr*

[b]*Research Center of Bioconvergence Analysis, Korea Basic Science Institute (KBSI), Ochang, Chungbuk 28119, Republic of Korea. E-mail: mr0505@kbsi.re.kr*

[c]*Department of Chemistry Education, Kongju National University, Gongju 32588, Republic of Korea*

[d]*Department of Chemistry, Ulsan National Institute of Science and Technology (UNIST), Ulsan 44919, Republic of Korea*

[e]*Research Headquarters, Korea Brain Research Institute (KBRI), Daegu 41068, Republic of Korea*

[f]*Bio-Analytical Science, University of Science and Technology (UST), Daejeon 34113, Republic of Korea*

[g]*Graduate School of Analytical Science and Technology, Chungnam National University, Daejeon 34134, Republic of Korea*

† Electronic supplementary information (ESI) available: Experimental section and Fig. S1–S16. See DOI: 10.1039/d0sc04366d

‡ These authors contributed equally to this work.

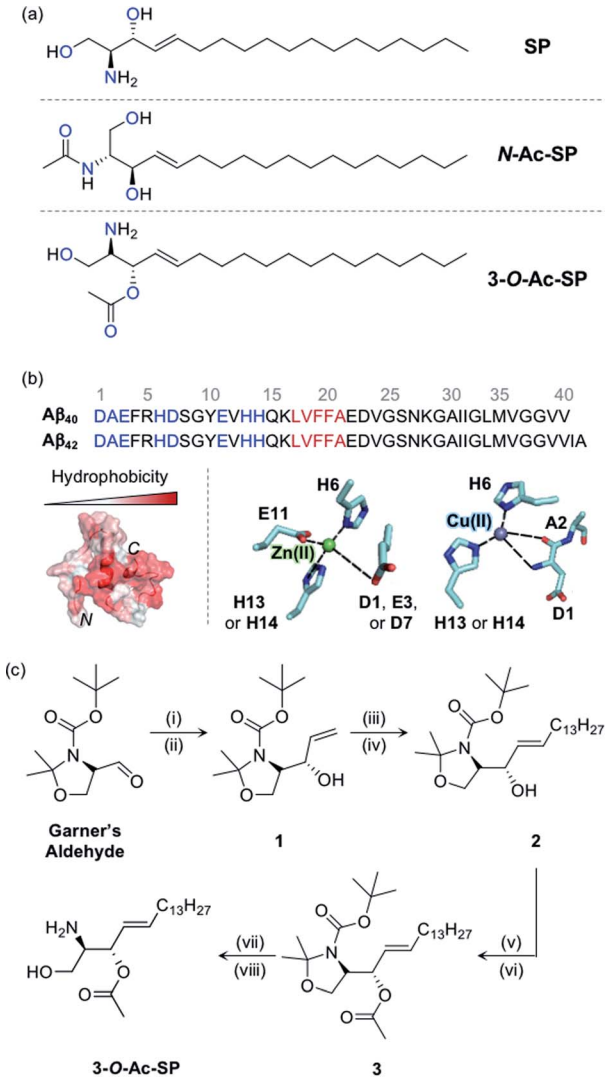

Fig. 1 SP and acetylsphingosines studied in this work. (a) Chemical structures of SP, *N*-Ac-SP, and 3-*O*-Ac-SP. An acetyl group was incorporated into the structure of SP at the *N*- or 3-*O*-position yielding *N*-Ac-SP and 3-*O*-Ac-SP, respectively. SP, (2*S*,3*R*)-2-amino-octadec-4-*trans*-ene-1,3-diol; *N*-Ac-SP, (2*S*,3*R*,4*E*)-2-(acetylamino)-4-octadecene-1,3-diol; 3-*O*-Ac-SP, (2*S*,3*S*,*E*)-2-amino-1-hydroxyoctadec-4-en-3-yl acetate. Potential donor atoms for metal binding are highlighted in blue. (b) Amino acid sequences of $A\beta_{40}$ and $A\beta_{42}$ (top) as well as hydrophobicity and metal binding of Aβ (bottom). Top: the amino acid residues involved in metal coordination and the self-recognition site are highlighted in blue and red, respectively. Bottom: (left) structure of $A\beta_{40}$ (PDB ID: 2LFM)[35] exhibiting a degree of hydrophobicity; (right) examples of Zn(II) and Cu(II) coordination to Aβ.[30,31] Possible fifth ligands on the metal centers are not shown in this figure. (c) Synthetic routes to 3-*O*-Ac-SP. Reagents and conditions: (i) (1) vinylmagnesium bromide, THF, −30 °C (30 min) to 0 °C (1 h); (ii) (2) sat. NH_4Cl (aq); (iii) 1-pentadecene, second-generation Grubbs catalyst; (iv) CH_2Cl_2, room temperature, 16 h; (v) acetyl chloride, 4-dimethylaminopyridine; (vi) pyridine : CH_2Cl_2 (2 : 1), room temperature, overnight; (vii) trifluoroacetic acid; (viii) CH_2Cl_2 : H_2O (2 : 1), room temperature, overnight.

pro-apoptotic conditions contributing towards neurodegeneration.[6,21,22] Recently, elevated concentrations of **SP** have been detected in the post-mortem brains of Alzheimer's disease (AD) patients.[22] Despite such notions, a connection between **SP** and AD is only beginning to be revealed.

AD is the most common neurodegenerative disease exhibiting significant intricacy in its pathology involving several pathogenic features, such as proteopathy and metal ion dyshomeostasis.[23–34] The proteopathic implications of AD include the pathology of amyloid-β (Aβ), while the metal ion hypothesis focuses on the dualistic pathogenic qualities of loss-of-function and gain-of-toxicity through metal ion dyshomeostasis and miscompartmentalization.[23–34] Increasing evidence indicates the independent and synergistic contributions of Aβ and metal ions towards neurodegeneration.[23–34] Aβ, the main component of senile plaques, is an aggregation-prone peptide that forms neurotoxic species.[24–35] Metal ions [*e.g.*, Zn(II) and Cu(II)] colocalized with Aβ aggregates in senile plaques can coordinate to Aβ peptides, as displayed in Fig. 1b, and affect the aggregation of Aβ.[24–34] The contemporary viewpoint on the complex pathology of AD considers the inter-relationships among different pathological elements found in the disease.[24,25,32]

In this study, **SP** was hypothesized to interact with Aβ and metal ions and subsequently alter the aggregation and cytotoxicity of metal-free Aβ and metal-bound Aβ (metal–Aβ). Such interactions under pathological conditions are supported by four fundamental aspects: (i) potential points of convergence at the subcellular level for **SP**, Aβ, and metal ions,[7,18,19,36] (ii) enhanced concentrations of **SP**, Aβ, and metal ions in AD-affected brains,[22,24–26] (iii) amphiphilic properties of both **SP** and Aβ, and (iv) inclusion of potential metal-binding sites on the structure of **SP**. Three sphingolipids, including **SP**, *N*-acetylsphingosine (***N*-Ac-SP**), and 3-*O*-acetylsphingosine (**3-*O*-Ac-SP**) shown in Fig. 1a, were utilized to experimentally confirm these interactions at the molecular level in association with their ability to form micelles and micellar aggregates and evaluate their impact on the aggregation and cytotoxicity of both metal-free Aβ and metal–Aβ. Overall, we provide a multidisciplinary perspective on the interactions and pathogenic connections between our molecular subjects.

Results and discussion

Preparation and properties of SP and acetylsphingosines

SP, a skeletal structure of sphingolipids, is subject to a diverse range of structural variations such as acylation, phosphorylation, and glycosylation, often serving as a measure to control cellular signaling.[5,12,37] In particular, acylation is a universal modification of biomolecules with nitrogen (N) and oxygen (O) atoms generating amide and ester groups, respectively.[38] In this work, we incorporated the acetyl functionality, as the simplest acyl group, onto the structure of **SP** to construct ***N*-Ac-SP** and **3-*O*-Ac-SP**, as presented in Fig. 1a, and employed them as representative sphingolipids, along with **SP**. **SP** and ***N*-Ac-SP** were obtained commercially, while **3-*O*-Ac-SP** was synthesized following previously reported procedures with slight modifications, as summarized in Fig. 1c.[39–43] The Grignard reaction of Garner's aldehyde with vinylmagnesium bromide produced **1**. Next, **2** was generated *via* the cross-metathesis reaction of **1** with 1-pentadecene using the second-generation Grubbs' catalyst. The subsequent

acetylation of **2** with acetyl chloride under basic conditions afforded **3**. Lastly, after acid-catalyzed deprotection of the cyclic *N*,*O*-aminal and *tert*-butoxycarbonyl group in **3**, the final product, **3-*O*-Ac-SP**, was obtained in a modest yield (Fig. S1†).

SP and the two acetylsphingosines are expected to interact with Aβ and metal ions based on their molecular structures depicted in Fig. 1a. For Aβ interaction, the alkenyl chains and the amino alcohol moieties with or without acetyl substitution of these molecules may interact with the hydrophobic and hydrophilic regions of Aβ, respectively, as presented in Fig. 1b.[26] All three compounds embody potential metal-binding sites. **SP** has two bidentate sites for metal ions, *i.e.*, the moieties of 2-aminoethanol and 1,3-propanediol. The two acetylsphingosines also have possible metal-binding sites composed of N and O donor atoms. Moreover, the amphiphilicity of these compounds drives their self-aggregation into micelles and micellar aggregates at concentrations above their CACs.[13–17] Their corresponding CACs were measured by dynamic light scattering in appropriate buffered solutions. The CACs of **SP**, ***N*-Ac-SP**, and **3-*O*-Ac-SP** were determined to be *ca.* 3–81 μM, 7–27 μM, and 29–68 μM, respectively, depending on pH and the presence of a salt (*e.g.*, NaCl) (Fig. S2†). The aggregation is initiated at their corresponding CACs. The concentration ratio of micelles and micellar aggregates to monomers theoretically increases in a manner proportional to their concentrations above the CACs.[44,45]

Interactions of SP and acetylsphingosines with Aβ

To analyze the molecular-level interactions between **SP**, ***N*-Ac-SP**, or **3-*O*-Ac-SP** and Aβ, binding studies were conducted by

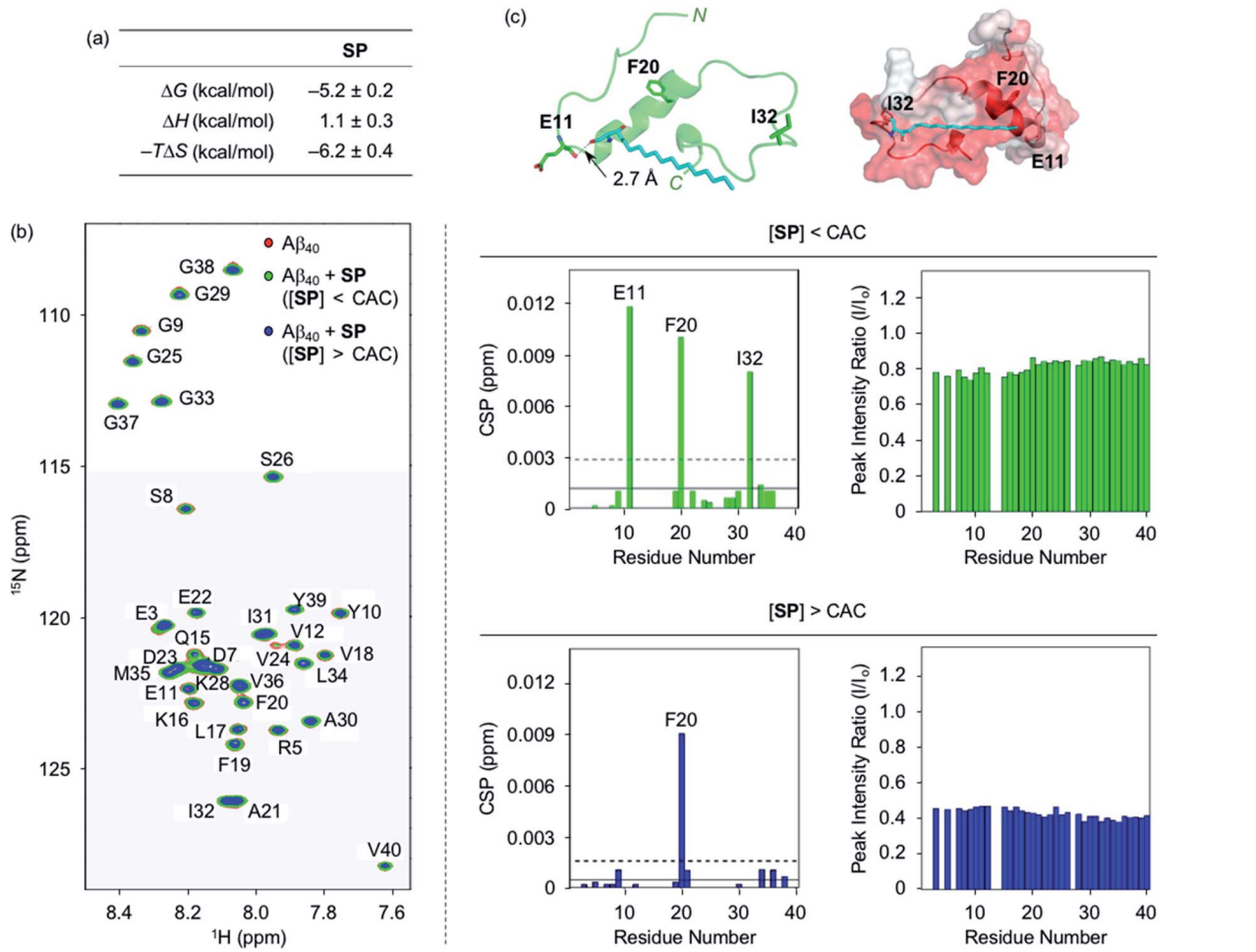

Fig. 2 Interactions of **SP** with Aβ. (a) Thermodynamic parameters for binding of **SP** to $A\beta_{40}$ determined by ITC. ITC data are shown in Fig. S3.† Conditions: [$A\beta_{40}$] = 500 μM; [**SP**] = 200 μM (1% v/v DMSO); 20 mM HEPES, pH 7.4; 10 °C. (b) 2D $^{1}H-^{15}N$ SOFAST-HMQC NMR analysis of the samples containing **SP** and ^{15}N-labeled $A\beta_{40}$. The spectra (left), CSPs (middle), and peak intensity ratios (right) of ^{15}N-labeled $A\beta_{40}$ were acquired upon addition of **SP** at the concentrations below or above the CAC. Two horizontal lines represent the average chemical shift (solid line) plus one standard deviation (dashed line). Conditions: [^{15}N-labeled $A\beta_{40}$] = 40 μM; [**SP**] = 2 μM (below the CAC) or 100 μM (above the CAC) (1% v/v DMSO); 20 mM HEPES, pH 7.4; 10% v/v D_2O; 10 °C. (c) Possible interactions between **SP** (cyan) and $A\beta_{40}$ monomer (PDB ID: 2LFM)[35] visualized by docking studies [cartoon (left) and surface (right) versions]. The amino acid residues in $A\beta_{40}$ with relatively large CSPs observed from the NMR studies are depicted in stick representation (left). The dashed line indicates possible hydrogen bonding between **SP** and $A\beta_{40}$ monomer within 3.0 Å. Hydrophobic contacts of **SP** onto the self-recognition site and the *C*-terminal region of $A\beta_{40}$ monomer are observed (right). Hydrophilic to hydrophobic amino acid residues are indicated in a gradient from white to red.

isothermal titration calorimetry (ITC) and two-dimensional band selective optimized flip-angle short transient-heteronuclear multiple quantum correlation nuclear magnetic resonance (2D SOFAST-HMQC NMR) spectroscopy. To avoid undesired aggregation of Aβ during experiments, we employed $Aβ_{40}$ that has a lower aggregation propensity than $Aβ_{42}$.[26,29,32,33] The concentration greater than the compounds' CACs was used for ITC experiments. Under these conditions, changes in heat were measured upon titrating $Aβ_{40}$ into the solutions of **SP**, ***N*-Ac-SP**, and **3-*O*-Ac-SP** to avoid their conformational transformations from the mixture of micelles and micellar aggregates to monomers that can induce heat changes during the titrations.[46] For the association of **SP** with Aβ, an endothermic isotherm was recorded with negative Gibbs free energy change (ΔG) displaying the spontaneous complex formation with an energetically unfavorable enthalpic contribution [*i.e.*, positive enthalpy change (ΔH)], as illustrated in Fig. 2a and S3.† The data suggested that interactions between the titrand and the titrant were thermodynamically favored by positive entropy change (ΔS) and could be mainly driven by hydrophobic interactions based on the greater contribution of entropy over enthalpy. It should be noted that the dissociation constant (K_d) of **SP** for Aβ could not be accurately determined due to its heterogeneous population in solution, including monomers, micelles, and micellar aggregates.

Moving forward, the interactions between **SP** and Aβ were further probed in detail by 2D SOFAST-HMQC NMR spectroscopy. As depicted in Fig. 2b, chemical shift perturbations (CSPs) were monitored when ^{15}N-labeled $Aβ_{40}$ was incubated with **SP** at concentrations below and above the CAC. The **SP**-induced CSPs for ^{15}N-labeled $Aβ_{40}$ were mostly moderate in magnitude suggesting weak and nonspecific interactions between the compound and Aβ. The E11, F20, I32, and F20 residues were subject to greater CSPs by treatment of the compound at concentrations below and above the CAC, respectively. Furthermore, the intensity of all amino acid residues was reduced upon the addition of **SP** to ^{15}N-labeled $Aβ_{40}$, which implies that **SP** may mediate the production of NMR-invisible Aβ aggregates.[47] Possible interactions between **SP** and the amino acid residues in $Aβ_{40}$ presenting relatively significant CSPs were visualized by docking studies employing the monomeric structure of $Aβ_{40}$ (PDB ID: 2LFM) that was identified by NMR in aqueous solution.[35] As shown in Fig. 2c, **SP** was simulated to form hydrogen bonding (*i.e.*, an O–H moiety of **SP** with the backbone carbonyl group between E11 and V12) and be positioned near the hydrophobic region of Aβ. The end of **SP**'s hydrocarbon chain was positioned near the self-recognition site responsible for driving Aβ aggregation.[24,29]

Interactions between the two acetylsphingosines and Aβ exhibited spontaneous complexation showing an endothermic process with the preferential entropic contributions compensating the unfavorable enthalpic contributions, as displayed in Fig. 3a and S4.† In a manner similar to **SP**, the interactions of ***N*-Ac-SP** and **3-*O*-Ac-SP** with Aβ may be primarily directed by hydrophobic interactions. Interestingly, the magnitude of entropic contributions seemed to increase in the order of **SP**, ***N*-Ac-SP**, and **3-*O*-Ac-SP**, while that of enthalpic contributions was in reverse order. This may suggest that the acetylsphingosines are more involved in the exclusion of water molecules from the surface of Aβ, relative to **SP**, facilitating their hydrophobic interactions with Aβ. It should be noted that the accurate K_d values of the acetylsphingosines for Aβ were not able to be obtained due to their heterogeneous conformations in solution at concentrations above the CACs. Based on the comparable ΔG values for the association of **SP** or the acetylsphingosines towards Aβ, which are logarithmically related to their K_d values, their binding affinities for Aβ are speculated to be in a similar range. As presented in Fig. 3b and S5,† 2D ^{1}H–^{15}N SOFAST-HMQC NMR studies revealed relatively low but detectable CSPs of several amino acid residues in ^{15}N-labeled $Aβ_{40}$ upon incubation with the acetylsphingosines (*e.g.*, F20, G29, and I32 for ***N*-Ac-SP** and G29 for **3-*O*-Ac-SP** at the concentrations below the CACs; E11, F20, G29, and I32 for ***N*-Ac-SP** and F20 and G29 for **3-*O*-Ac-SP** at the concentrations above the CACs). These observations indicate weak and nonspecific interactions of both ***N*-Ac-SP** and **3-*O*-Ac-SP** towards Aβ. No notable decrease in the overall peak intensity of ^{15}N-labeled $Aβ_{40}$ was observed by treatment of the acetylsphingosines. Moreover, docking studies indicated that both acetylsphingosines were situated on the hydrophobic region of $Aβ_{40}$ pertaining to the amino acid residues that exhibited relatively significant CSPs from 2D NMR studies, as shown in Fig. 3c. The hydrophobic interactions at the self-recognition site of $Aβ_{40}$ were visualized with the ends of hydrocarbon chains of the two acetylsphingosines. Taken together, the ITC and 2D NMR studies demonstrate that **SP** and the acetylsphingosines, in either their monomeric or micellar forms, can directly interact with Aβ, with the support of docking studies.

Metal-binding properties of SP and acetylsphingosines in the absence and presence of Aβ

To assess whether **SP**, ***N*-Ac-SP**, and **3-*O*-Ac-SP** can bind to metal ions in aqueous media, titration experiments with Zn(II) and Cu(II) were performed using ^{1}H NMR and UV-visible (UV-vis) spectroscopy, respectively. It should be noted that potential metal-binding moieties in the structure of **SP**, *i.e.*, 2-aminoethanol and 1,3-propanediol, were used for these studies due to its limited aqueous solubility.[48] When Zn(II) was added to a solution of 2-aminoethanol, the peaks assigned to the α-protons became deshielded in the NMR spectra, as illustrated in Fig. 4a. This observation could be explained by the lower electron density of 2-aminoethanol upon binding to Zn(II). Moreover, our titration measurements further estimated the K_d value of **SP** towards Zn(II) to be in the micromolar range under our experimental conditions. In the case of 1,3-propanediol, the K_d value for Zn(II) could not be determined although excess amounts of Zn(II) were titrated into the solution of the ligand (data not shown). As expected from the hard and soft acid and base concept[49] and the size of chelate rings,[50] Zn(II) chelation of 2-aminoethanol, with N and O donor atoms forming a five-membered chelate ring, was more favorable than that of 1,3-propanediol containing two O donor atoms to generate a six-membered chelate ring. Thus, Zn(II) binding of **SP** can occur

(a)

	ΔG (kcal/mol)	ΔH (kcal/mol)	−TΔS (kcal/mol)
***N*-Ac-SP**	−5.2 ± 0.2	5.2 ± 0.7	−10.4 ± 0.7
3-*O*-Ac-SP	−5.3 ± 0.1	7.2 ± 0.3	−12.5 ± 0.3

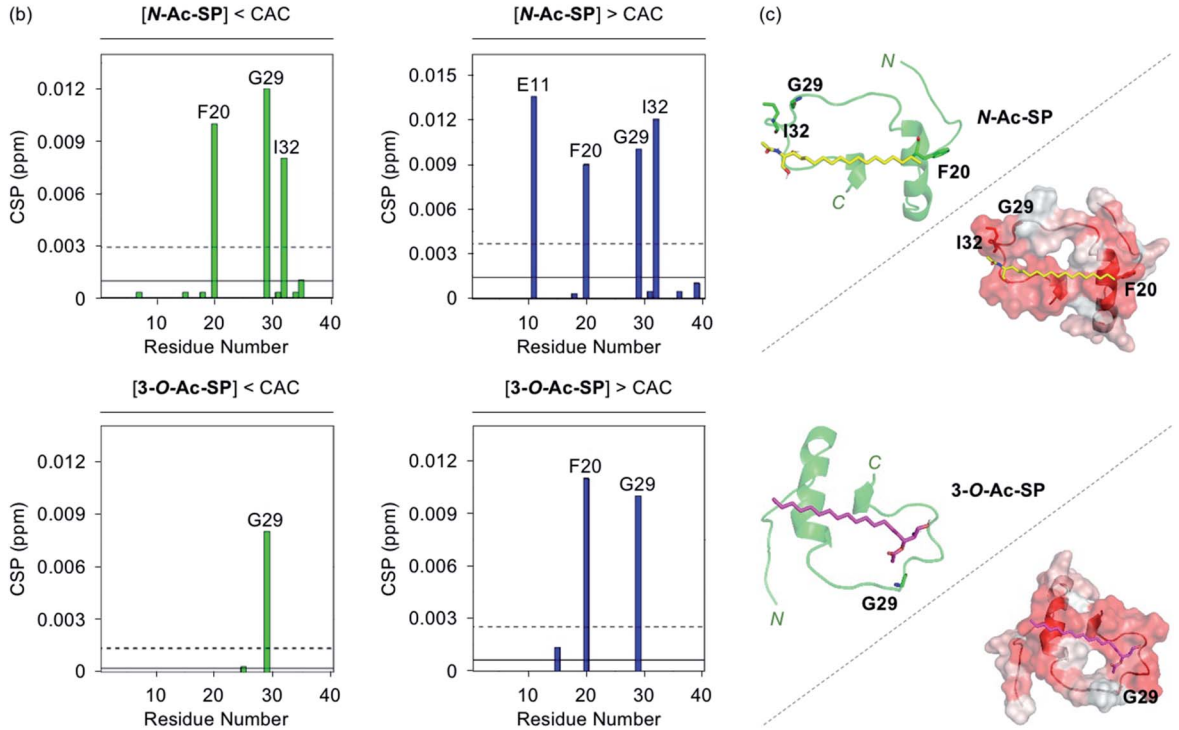

Fig. 3 Interactions of ***N*-Ac-SP** and **3-*O*-Ac-SP** with Aβ monomer. (a) Thermodynamic parameters for binding of ***N*-Ac-SP** and **3-*O*-Ac-SP** to $A\beta_{40}$ measured by ITC. ITC data are shown in Fig. S4.† Conditions: $[A\beta_{40}] = 500$ μM; [acetylsphingosine] = 200 μM (1% v/v DMSO); 20 mM HEPES, pH 7.4; 10 °C. (b) CSPs in $A\beta_{40}$ upon addition of ***N*-Ac-SP** and **3-*O*-Ac-SP** at the concentrations below or above their CACs obtained from 2D $^{1}H-^{15}N$ SOFAST-HMQC NMR spectra (Fig. S5†). Average CSPs (solid line) are indicated with standard deviations (dashed line). Conditions: [^{15}N-labeled $A\beta_{40}$] = 40 μM; [compound] = 2 μM (below the CAC) or 100 μM (above the CAC) (1% v/v DMSO); 20 mM HEPES, pH 7.4; 10% v/v D_2O; 10 °C. (c) Possible conformations of ***N*-Ac-SP** (yellow) and **3-*O*-Ac-SP** (pink) docked with $A\beta_{40}$ monomer (PDB ID: 2LFM)[35] [cartoon (left) and surface (right) versions]. The amino acid residues in $A\beta_{40}$ with relatively large CSPs are presented in stick representation (left). Hydrophobic contacts of the acetylsphingosines onto the self-recognition site and the *C*-terminal region of $A\beta_{40}$ monomer are displayed (right). Hydrophilic to hydrophobic amino acid residues are indicated in a gradient from white to red.

preferentially *via* the 2-aminoethanol moiety. The metal-binding properties of the acetylsphingosines were also considered with their potential metal-binding sites (*i.e.*, 1,3-propanediol for ***N*-Ac-SP**; 2-aminoethanol for **3-*O*-Ac-SP** shown in Fig. 1a). ***N*-Ac-SP** includes the *N*-(2-hydroxyethyl)acetamide group as an additional site for possible metal binding. Unfortunately, the K_d value of this moiety for Zn(II) could not be obtained even with excess concentrations of Zn(II) (data not shown). Therefore, **SP** and **3-*O*-Ac-SP** exhibit a greater Zn(II)-binding ability than ***N*-Ac-SP** through the 2-aminoethanol group.

Cu(II)-binding properties of 2-aminoethanol were analyzed *via* solution speciation studies with UV-vis variable-pH titrations. Spectrophotometric titrations of 2-aminoethanol (L) in the absence of Cu(II) were first performed to estimate its acidity constant (pK_a), as shown in Fig. S6.† The solution speciation diagram depicts the presence of neutral (L) and monoprotonated (LH) forms of 2-aminoethanol in the pH range from 3 to 11. At pH 6.8, a condition plausibly representing a physiologically acidotic environment where Aβ aggregation is suggested to be facilitated in the presence of Cu(II),[51] and at physiological pH (pH 7.4), the LH form of the ligand was predicted to be major. Employing the pK_a value [9.79(0)] of the ligand, solution speciation experiments in the presence of Cu(II) were further carried out to determine the Cu(II)-to-ligand stoichiometry and its binding affinity for Cu(II). As shown in Fig. 4b, Cu(II)–ligand complexes with 1 : 1 and/or 1 : 2 Cu(II)-to-ligand stoichiometry were indicated in the solution speciation diagram at pH 6.8 and pH 7.4. Moreover, the binding affinity of the ligand for Cu(II) was predicted based on the values of stability constants (log β) and pCu [$pCu = -\log[Cu_{free}]$, where $[Cu_{free}]$ indicates the concentration of unchelated Cu(II)]. Considering the protonation and complexation for 2-aminoethanol at the given pH and concentrations of the ligand and Cu(II), the value of pCu was obtained as indicative of the relative Cu(II)-binding ability of the ligand under experimental conditions.[52,53] 2-Aminoethanol exhibited the pCu values as 7.96 and 9.08 at pH 6.8 and pH 7.4, respectively, that are expected to be

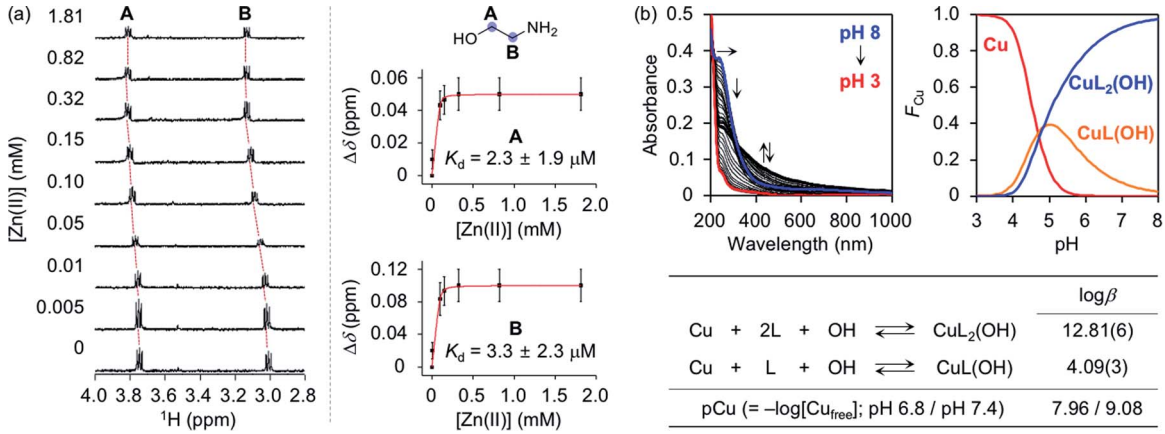

Fig. 4 Metal-binding properties of 2-aminoethanol. (a) ^{1}H NMR spectra (left) and changes in the chemical shifts ($\Delta\delta$; right) of 2-aminoethanol with various concentrations of Zn(II). Red curves were fitted to the $\Delta\delta$ values of the peaks assigned to the protons at the A and B positions to estimate a binding affinity of the compound for Zn(II). Error bars indicate the standard error from three independent experiments. Conditions: [2-aminoethanol] = 100 μM; [Zn(II)] = 0.005, 0.01, 0.05, 0.10, 0.15, 0.32, 0.82, and 1.81 mM; [DSS (2,2-dimethyl-2-silapentane-5-sulfonate sodium salt)] = 10 μM (internal reference); H_2O : D_2O (9 : 1). (b) Solution speciation studies of Cu(II)–2-aminoethanol (L) complexes. Top: UV-vis variable-pH titration spectra (left) and solution speciation diagram (right) were obtained by spectrophotometric titrations of Cu(II)–ligand complexes (F_{Cu} = fraction of species at given pH). Bottom: the values of log β and pCu of Cu(II)–ligand complexes were summarized in the table. The errors in the last digit are shown in parentheses. Charges are omitted for clarity. Conditions: [2-aminoethanol] = 400 μM; [Cu(II)] = 200 μM; room temperature; I = 0.10 M NaCl.

higher than pZn at each pH based on Irving–Williams series.[54] According to previously reported studies, Cu(II) in the solution of aminosugars and aminoglycosides containing aminoalcohol moieties has been observed to lower the pK_a of hydroxyl groups in the ligands, corroborating the higher binding affinity of 2-aminoethanol for Cu(II) than Zn(II).[55–57] It should be noted that the values of pCu for the 1,3-propanediol and *N*-(2-hydroxyethyl) acetamide moieties could not be obtained due to their insignificant optical changes upon addition of Cu(II) (data not shown). Overall, **SP** and **3-*O*-Ac-SP** can coordinate to Cu(II) through the 2-aminoethanol functionality. The comparable metal-binding affinities of 2-aminoethanol in **SP** and **3-*O*-Ac-SP** with those of Aβ [$K_d = 10^{-9}$ to 10^{-6} M for Zn(II)–Aβ at pH 7.4; $K_d = 10^{-6}$ to 10^{-12} M and pCu = *ca.* 6–12 for Cu(II)–Aβ in the pH range from 6.5 to 7.4][24,58] support their ability to competitively bind to metal ions with Aβ.

To evaluate whether **SP** containing the 2-aminoethanol group can chelate out the metal ion from metal–Aβ, its interaction with metal–Aβ was analyzed by 2D SOFAST-HMQC NMR and electron paramagnetic resonance (EPR) spectroscopy (Fig. 5, S7, and S8†). As depicted in Fig. 5b, the addition of Zn(II) into the solution of ^{15}N-labeled Aβ_{40} led to remarkable changes in the NMR signals of the amino acid residues in the *N*-terminal region. Particularly, the peaks of the amino acid residues close to the Zn(II)-binding site in Aβ (Fig. 1b), *e.g.*, R5, D7, S8, G9, E11, and V12, disappeared, indicative of Zn(II) binding to Aβ.[59,60] When **SP** at the concentration above its CAC was introduced into the solution of ^{15}N-labeled Aβ_{40} in the presence of Zn(II), the peak signals corresponding to most of the aforementioned amino acid residues were restored to certain extents. This suggests that Zn(II) binding to Aβ could be partially disrupted by **SP**. ***N*-Ac-SP**, which does not include the 2-aminoethanol moiety, was not able to affect binding of Zn(II) to Aβ at the concentration above its CAC (Fig. S9†), as expected from its relatively poor metal-binding ability. It should be noted that the ability of the compounds at concentrations below their CACs to chelate out Zn(II) from Zn(II)–Aβ could not be distinguishably detected under our experimental conditions (*i.e.*, [^{15}N-labeled Aβ_{40}] = 40 μM; [compound] = 2 μM), as presented in Fig. S10 and S11.† Overall, **SP** with its micellar species potentially sequesters Zn(II) from Zn(II)–Aβ, which is expected based on the Zn(II)-binding affinity of 2-aminoethanol in **SP** (Fig. 4a).

The interaction of **SP** with Cu(II)–Aβ at the concentration above its CAC was examined by EPR spectroscopy. For the EPR studies, Aβ_{16}, an *N*-terminal fragment of full-length Aβ that binds to metal ions and shows no significant aggregation,[24] was used. Upon treatment of **SP** into the solution of Cu(II), the shifts in symmetry of the *g*- and *A*-values were observed from axial to isotropic, as depicted in Fig. 5c and S8,† suggesting its binding to Cu(II). This is expected from the Cu(II)-binding affinity of 2-aminoethanol (Fig. 4b). The sample of Cu(II) with Aβ_{16} produced an axial EPR signal at $g_\perp = 2.05$ and $g_\parallel = 2.28$ with the hyperfine splitting of $A_\perp = 6.96$ G and $A_\parallel = 167.75$ G (Fig. 5c and S8†), indicative of the complexation between Cu(II) and Aβ_{16}.[61] When **SP** was added into the solution containing Cu(II) and Aβ_{16}, the EPR spectrum was different from that of the Cu(II) samples with either **SP** or Aβ_{16}. Cu(II) binding was further quantified by weighted summation of the normalized spectra of the Cu(II) samples containing either Aβ_{16} or **SP** following the previously reported procedure.[62–64] As a result, the EPR spectrum of the Cu(II) sample treated with both Aβ_{16} and **SP** exhibited a mixture of Cu(II) bound to **SP** (10%) and Aβ_{16} (90%). Thus, the EPR studies demonstrate the ability of **SP** to potentially chelate out Cu(II) from Cu(II)–Aβ. In contrast, the EPR spectra for the Cu(II) samples with ***N*-Ac-SP** in the absence and presence of Aβ_{16} were almost identical with those of compound-free Cu(II) samples

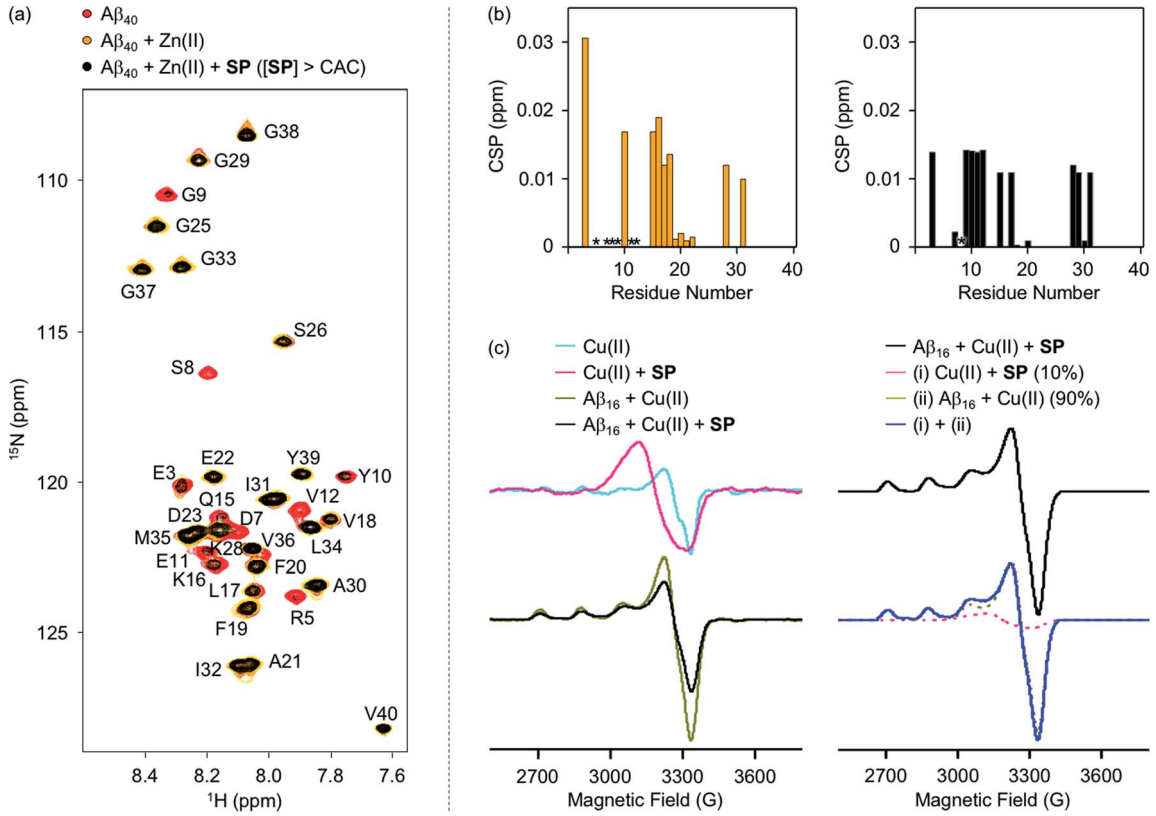

Fig. 5 Interactions of **SP** with metal–Aβ analyzed by 2D ^{1}H–^{15}N SOFAST-HMQC NMR and EPR spectroscopy. (a) 2D NMR spectra of ^{15}N-labeled $A\beta_{40}$ with and without Zn(II) and **SP** at the concentration above the CAC. (b) CSPs of the Zn(II) samples in the absence (left) and presence (right) of **SP** at the concentration above the CAC. Upon addition of Zn(II) to the solution of ^{15}N-labeled $A\beta_{40}$ with and without **SP**, the NMR signals of the amino acid residues indicated in asterisks (*) disappeared. Conditions: [^{15}N-labeled $A\beta_{40}$] = 40 μM; [Zn(II)] = 40 μM; [**SP**] = 100 μM (above the CAC) (1% v/v DMSO); 20 mM HEPES, pH 7.4; 10% v/v D_2O; 10 °C. (c) EPR spectra of the Cu(II) samples with and without **SP** and $A\beta_{16}$. The simulated spectrum (blue), similar to the normalized experimental spectrum of the Cu(II) sample with $A\beta_{16}$ and **SP** (black), was obtained by weighted summation of the normalized spectra of the Cu(II) samples with either **SP** (10%; pink) or $A\beta_{16}$ (90%; dark yellow). Conditions: [$A\beta_{16}$] = 100 μM; [Cu(II)] = 100 μM; [**SP**] = 400 μM (above the CAC) (1% v/v DMSO); 20 mM HEPES, pH 6.8, 150 mM NaCl; 37 °C; 24 h; constant agitation. The EPR spectra were collected with the following experimental parameters: microwave frequency, 9.41 GHz; microwave power, 2 mW; modulation frequency, 100 kHz; modulation amplitude, 10 G; time constant, 0.01 ms; conversion time, 60 ms; sweep time, 120 s; number of scan, 4; temperature, 100 K.

with and without $A\beta_{16}$ (Fig. S8 and S12†), indicating that this compound cannot significantly affect Cu(II) coordination to Aβ. These distinct behaviors of the compounds against metal–Aβ at the concentrations above their CACs are also supported by the previous studies displaying that ionic micelles can induce structural changes of peptides and proteins in a manner affecting their Cu(II)-binding properties.[65–67] Taken together, as expected from the compounds' metal-binding affinities, the spectroscopic studies manifest that **SP** potentially sequesters the metal ion from metal–Aβ.

Influence of SP and acetylsphingosines on the aggregation of metal-free and metal-associated Aβ

The effects of **SP**, ***N*-Ac-SP**, and **3-*O*-Ac-SP**, at concentrations below and above the CACs, on the aggregation of $A\beta_{40}$ and $A\beta_{42}$ with and without Zn(II) and Cu(II) were evaluated. Upon incubation of **SP** with freshly prepared metal-free and metal-treated Aβ, as displayed in Fig. 6, S14, and S15,† the size distribution and the morphology of the resultant Aβ species were analyzed by gel electrophoresis with western blotting (gel/Western blot) and transmission electron microscopy (TEM), respectively. Aβ species with molecular weights (MWs) in a range from *ca.* 4 kDa (monomer) to *ca.* 240 kDa (aggregate) can be probed as visible bands in gel/Western blot.[68] In particular, the smearing bands from compound-treated Aβ samples, distinct from compound-free Aβ samples, indicate that the compound can vary Aβ aggregation. Aβ aggregates that are too large to penetrate the gel matrix can be visualized by TEM.

At the concentration below the CAC, **SP** did not significantly affect the aggregation of metal-free $A\beta_{42}$, as shown in Fig. 6b. In the case of Zn(II)–$A\beta_{42}$ incubated with **SP**, however, more intense bands were detected at *ca.* 25 kDa with the MW range larger than *ca.* 50 kDa, relative to compound-untreated Zn(II)–$A\beta_{42}$. The sample of Cu(II)–$A\beta_{42}$ treated with **SP** indicated an increase in the levels of dodecameric or larger $A\beta_{42}$ species (*ca.* ≥50 kDa), compared to that of compound-free Cu(II)–$A\beta_{42}$. Upon increasing the concentration of **SP** beyond the CAC, changes in the MW distributions of $A\beta_{42}$ became more dramatic, showing

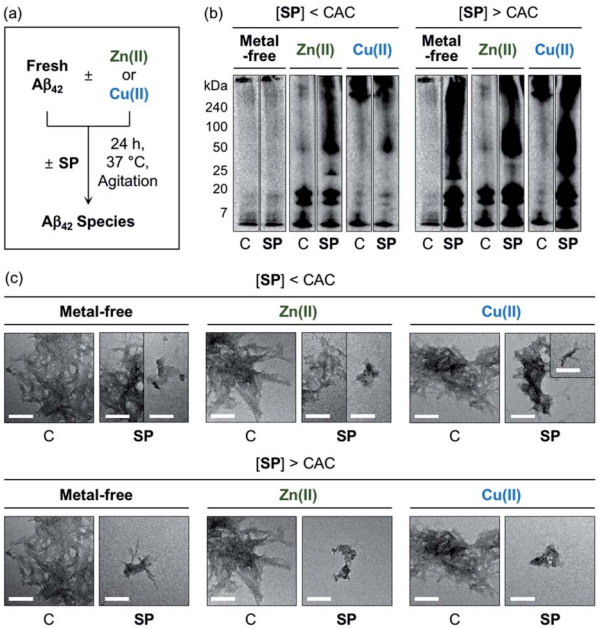

Fig. 6 Impact of SP on metal-free and metal-induced $A\beta_{42}$ aggregation. (a) Scheme of $A\beta_{42}$ aggregation experiments. (b) Analysis of the size distribution of the resultant $A\beta_{42}$ species by gel/Western blot using an anti-Aβ antibody (6E10). Lanes: (C) $A\beta_{42} \pm Zn(II)$ or $Cu(II)$; (SP) C + SP. The original gel images are shown in Fig. S13.† (c) Morphologies of the resultant $A\beta_{42}$ aggregates from (b) detected by TEM. Conditions: $[A\beta_{42}] = 25$ μM; [Zn(II) or Cu(II)] = 25 μM; [compound] = 10 μM (below the CAC) or 100 μM (above the CAC) (1% v/v DMSO); 20 mM HEPES, pH 7.4 [for metal-free and Zn(II)-containing samples] or pH 6.8 [for Cu(II)-containing samples], 150 mM NaCl; 37 °C; 24 h; constant agitation. Scale bars = 200 nm.

smearing bands at *ca.* 4–240 kDa for metal-free $A\beta_{42}$ and Cu(II)–$A\beta_{42}$. The intensity of the bands from the sample containing Zn(II)–$A\beta_{42}$ and **SP** was enhanced at *ca.* 4–20 kDa and above *ca.* 50 kDa.

In the TEM studies, as displayed in Fig. 6c, the incubation of **SP** with metal-free and metal-treated $A\beta_{42}$ resulted in the generation of $A\beta_{42}$ aggregates indicating a mixed morphology with both fibrillary and amorphous characteristics. The overall size of the aggregate species was reduced with the treatment of **SP**, compared to those of the compound-free samples. At the concentration above the CAC, the **SP**-induced changes in the sizes of $A\beta_{42}$ aggregates became more prominent, forming remarkably smaller Aβ species. Based on these observations, **SP** was demonstrated to modulate the aggregation of both metal-free and metal-treated $A\beta_{42}$ and such reactivities were further intensified with its micellar species. The results of gel/Western blot and TEM studies with metal-free $A\beta_{40}$ and metal–$A\beta_{40}$ showed lacking reactivity from the samples incubated with **SP** at the concentration below the CAC (Fig. S14†). At the concentration above the CAC, **SP** altered the aggregation of metal-free $A\beta_{40}$ and Cu(II)–$A\beta_{40}$, but it did not significantly affect Zn(II)–$A\beta_{40}$ aggregation. As shown in the ITC and 2D NMR studies (*vide supra*), hydrophobic interactions between **SP** and Aβ may promote the effect of the compound on the formation of Aβ aggregates. The metal-binding properties of **SP** could further support its ability to change the aggregation of metal–Aβ. In particular, the capability of **SP** at concentrations above the CAC to partially sequester the metal ion from metal–Aβ is expected to contribute to its reactivity towards the aggregation of metal–Aβ. It is noteworthy that multiple interactions of **SP** with metal–Aβ at concentrations above the CAC are possible based on the observations and findings through the NMR and EPR studies. For example, the transient ternary complexation between metal–Aβ and **SP** and the interactions of metal-free and/or metal-bound **SP** with the hydrophobic core and *C*-terminal region of Aβ (Fig. S7†) could simultaneously occur, along with metal displacement by **SP**. These could result in the modulative impact of **SP** with its micellar species on the aggregation of metal–Aβ.

The generation of Aβ aggregates in the presence of ***N*-Ac-SP** and **3-*O*-Ac-SP** was further analyzed (Fig. 7). At the concentrations under the CACs, ***N*-Ac-SP** produced new bands larger than *ca.* 25 kDa or 50 kDa for the samples of metal-free $A\beta_{42}$ and metal–$A\beta_{42}$, as depicted in Fig. 7b. When **3-*O*-Ac-SP** was treated to metal-free $A\beta_{42}$ and metal–$A\beta_{42}$, the amount of aggregates with MW larger than *ca.* 50 kDa was increased, along with that of hexameric species at *ca.* 25 kDa, under metal-free and Zn(II)-present conditions. At the concentrations above the CACs, ***N*-Ac-SP** noticeably varied the MW distributions larger than *ca.* 25 kDa for metal-free $A\beta_{42}$, 7–25 kDa and above *ca.* 100 kDa for Zn(II)–$A\beta_{42}$, and 7–240 kDa for Cu(II)–$A\beta_{42}$. In the case of **3-*O*-Ac-SP**, a new smearing band in the MW range larger than *ca.* 25 kDa was detected from metal-free $A\beta_{42}$, while that with MW larger than *ca.* 50 kDa was observed for metal–$A\beta_{42}$. In particular, the treatment of **3-*O*-Ac-SP** with Cu(II)–$A\beta_{42}$ led to the detection of a band at *ca.* 25 kDa. The TEM studies revealed that both ***N*-Ac-SP** and **3-*O*-Ac-SP** at the concentrations below their CACs fostered the production of smaller $A\beta_{42}$ aggregates, compared to compound-untreated metal-free $A\beta_{42}$ and metal–$A\beta_{42}$, as presented in Fig. 7c. Upon addition of the acetylsphingosines at the concentrations above their CACs, relative to compound-free peptide samples, smaller aggregates of $A\beta_{42}$ were exhibited with a mixture of morphologies with filamentous or amorphous qualities in the absence and presence of metal ions. As shown in Fig. S15,† the acetylsphingosines did not discernably influence the aggregation of metal-free and metal-treated $A\beta_{40}$. Overall, **SP**, ***N*-Ac-SP**, and **3-*O*-Ac-SP** are capable of modifying Aβ aggregation in the absence and presence of metal ions to distinct degrees at concentrations below and above their CACs.

Impact of SP and acetylsphingosines on the toxicity induced by metal-free Aβ and metal–Aβ in living cells

Prior to cell studies with metal-free and metal-treated Aβ, the cytotoxicity of **SP**, ***N*-Ac-SP**, and **3-*O*-Ac-SP** was investigated by the MTT assay employing human neuroblastoma SH-SY5Y (5Y) cells [MTT = 3-(4,5-dimethylthiazol-2-yl)-2,5-diphenyltetrazolium bromide]. The half-maximal inhibitory concentration (IC_{50}) values for **SP** and ***N*-Ac-SP** were determined to be in the micromolar range, as summarized in Fig. S16a.† The IC_{50} value for **3-*O*-Ac-SP** could not be obtained under our

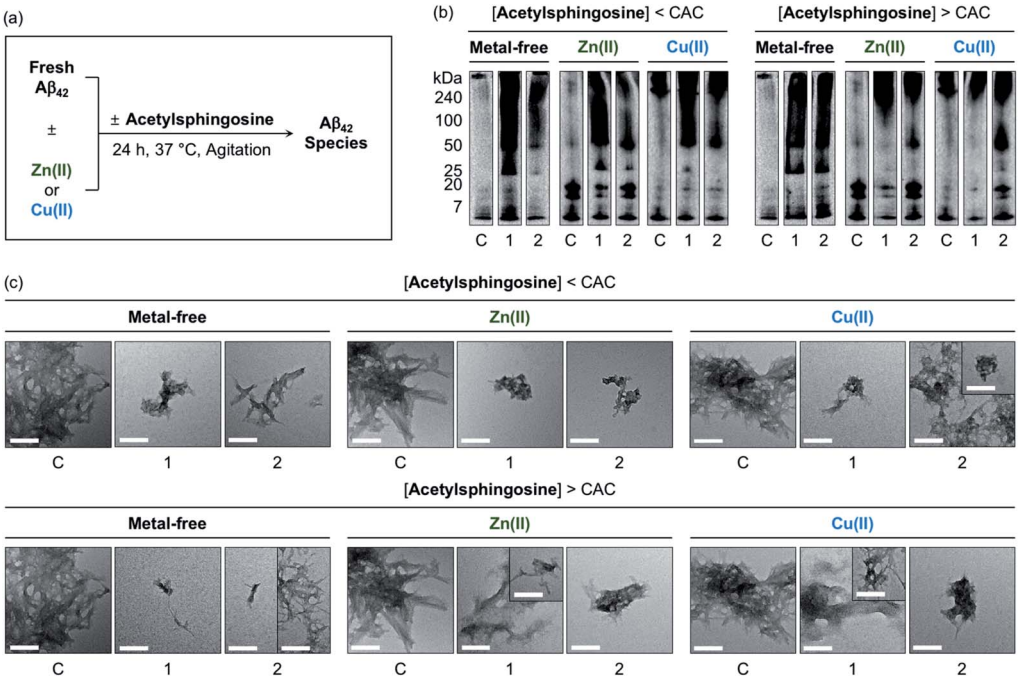

Fig. 7 Influence of *N*-Ac-SP and 3-*O*-Ac-SP on the aggregation of metal-free $A\beta_{42}$ and metal–$A\beta_{42}$. (a) Scheme of $A\beta_{42}$ aggregation experiments. (b) Analysis of the size distribution of the resultant $A\beta_{42}$ species by gel/Western blot using an anti-Aβ antibody (6E10). Lanes: (C) $A\beta_{42}$ ± Zn(II) or Cu(II); (1) C + *N*-Ac-SP; (2) C + 3-*O*-Ac-SP. The original gel images are shown in Fig. S13.† (c) Morphologies of the resultant $A\beta_{42}$ aggregates from (b) detected by TEM. Conditions: $[A\beta_{42}] = 25\ \mu M$; [Zn(II) or Cu(II)] = 25 μM; [acetylsphingosine] = 10 μM (below the CAC) or 100 μM (above the CAC) (1% v/v DMSO); 20 mM HEPES, pH 7.4 [for metal-free and Zn(II)-containing samples] or pH 6.8 [for Cu(II)-containing samples], 150 mM NaCl; 37 °C; 24 h; constant agitation. Scale bars = 200 nm.

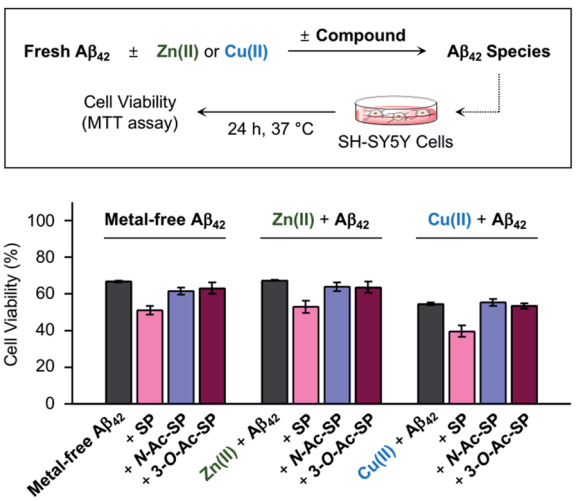

Fig. 8 Effect of SP, *N*-Ac-SP, and 3-*O*-Ac-SP on the toxicity induced by metal-free $A\beta_{42}$ or metal–$A\beta_{42}$ in living cells. Cell viability, determined by the MTT assay, was calculated in comparison to that of the cells treated with an equivalent amount of the buffered solution with 0.2% v/v DMSO (20 mM HEPES, pH 7.4 or pH 6.8, 150 mM NaCl). Error bars indicate the standard error from three independent experiments. Conditions: $[A\beta_{42}] = 10\ \mu M$; [Zn(II) or Cu(II)] = 10 μM; [compound] = 10 μM (0.2% v/v DMSO); 20 mM HEPES, pH 7.4 [for metal-free and Zn(II)-containing samples] or pH 6.8 [for Cu(II)-containing samples], 150 mM NaCl.

experimental conditions due to its relatively less toxicity (*ca.* >55% cell survival up to 100 μM). Moving forward, to examine the effects of **SP** and the acetylsphingosines on the cytotoxicity induced by $A\beta_{42}$ in the absence and presence of metal ions, the samples containing Aβ with either Zn(II) or Cu(II), a compound, or both were treated to 5Y cells, as shown in Fig. 8. The treatment of **SP** with metal-free and metal-treated $A\beta_{42}$ resulted in a further reduction in cell viability by *ca.* 15%. In contrast, when the cells were incubated with ***N*-Ac-SP** or **3-*O*-Ac-SP** with metal-free and metal–$A\beta_{42}$, the cell viabilities were not significantly affected. It should be noted that incubation of the compounds with 5Y cells at their concentrations used for cell studies with Aβ presented cell survival rates greater than *ca.* 80% in the absence and presence of Zn(II) or Cu(II) (Fig. S16b†). These results suggest that **SP**, but not ***N*-Ac-SP** and **3-*O*-Ac-SP**, may have a deteriorative impact on the toxicity induced by metal-free and metal-treated $A\beta_{42}$.

Conclusions

As the lipid membrane-mediated perturbations in the properties of Aβ come to the fore, lipidomics is emerging as an aspect of AD prompting the advancement of our knowledge towards the relevancy of lipids in its pathology.[26,69–74] AD-associated disturbances in the cerebral composition of sphingolipids, along with their neurobiological implications, suggest their potential roles in the progression of the disease.[21,22] In this

study, we first demonstrated that **SP** could bind to Aβ, mainly through hydrophobic interactions, and metal ions and consequently alter the aggregation of both metal-free Aβ and metal–Aβ. Moreover, the toxicity of metal-free Aβ and metal–Aβ in living cells was aggravated in the presence of **SP**. The acetylation of **SP** at *N*- and 3-*O*-positions resulted in more dominant hydrophobic interactions with Aβ, manifesting different degrees of the reactivity with metal-free Aβ and metal–Aβ. Additionally, the acetylsphingosines showed the diminished ability to vary the cytotoxicity of metal-free Aβ and metal–Aβ. Considering the aggregation of sphingolipids, we confirmed the distinct extents of modulative capacities towards the aggregation of metal-free $A\beta_{42}$ and metal–$A\beta_{42}$ depending on the presence of micellar **SP** or acetylsphingosines. Based on previously reported studies, micellar species can interact with Aβ in different manners from monomeric lipids (*e.g.*, the association of Aβ onto the surface of the membrane and the penetration of Aβ into the membrane).[69,73,75] Further mechanistic studies in consideration of the charge state of the compounds and the curvature of their micellar species, along with the aggregation state and spatiotemporal distribution of Aβ, would assist in gaining a better understanding of molecular-level interactions of sphingolipids with Aβ at concentrations below and above their CACs.[69,73,75–78] Collectively, this work illustrates that a single structural component of membranes, probably with its aggregated forms, can directly interact with the pathological components linked to AD and affect their properties and toxicity. Our overall findings can open new avenues for a molecular-level understanding of lipids with respect to their interactions and reactivities towards the pathological factors found in AD.

Conflicts of interest

There are no conflicts to declare.

Acknowledgements

This research is supported by the National Research Foundation of Korea (NRF) grants funded by the Korean government [NRF-2016R1A5A1009405 and NRF-2017R1A2B3002585 (M. H. L.); NRF-2018K1A3A1A39088040 and NRF-2019R1A2C1004954 (Y.-H. L.)]; the National Research Council of Science & Technology (NST) grant funded by the Korea government (MSIP) [CAP-17-05-KIGAM (Y.-H. L.)]. Y. Y. and J. H. thank the Global PhD fellowship program for support through the NRF funded by the Ministry of Education (NRF-2019H1A2A1075388 and NRF-2019H1A2A1073754 respectively). We thank Jong-Min Suh for assistancewith EPR studies.

Notes and references

1 C. Betsholtz, *Nat. Genet.*, 2015, **47**, 699.
2 H. A. Brown and R. C. Murphy, *Nat. Chem. Biol.*, 2009, **5**, 602.
3 A. H. Merrill, Jr, *Chem. Rev.*, 2011, **111**, 6387.
4 R. C. Murphy, J. Fiedler and J. Hevko, *Chem. Rev.*, 2001, **101**, 479.
5 Y. A. Hannun and L. M. Obeid, *Nat. Rev. Mol. Cell Biol.*, 2018, **19**, 175.
6 O. Cuvillier, G. Pirianov, B. Kleuser, P. G. Vanek, O. A. Coso, J. S. Gutkind and S. Spiegel, *Nature*, 1996, **381**, 800.
7 A. H. Futerman and Y. A. Hannun, *EMBO Rep.*, 2004, **5**, 777.
8 Y. H. Zeidan and Y. A. Hannun, *Trends Mol. Med.*, 2007, **13**, 327.
9 M. Trayssac, Y. A. Hannun and L. M. Obeid, *J. Clin. Invest.*, 2018, **128**, 2702.
10 G. D. Paolo and T.-W. Kim, *Nat. Rev. Neurosci.*, 2011, **12**, 284.
11 S. T. Pruett, A. Bushnev, K. Hagedorn, M. Adiga, C. A. Haynes, M. C. Sullards, D. C. Liotta and A. H. Merrill, Jr, *J. Lipid Res.*, 2008, **49**, 1621.
12 F. M. Goñi and A. Alonso, *Biochim. Biophys. Acta*, 2006, **1758**, 1902.
13 H. Sasaki, H. Arai, M. J. Cocco and S. H. White, *Biophys. J.*, 2009, **96**, 2727.
14 D. Reker, G. J. L. Bernardes and T. Rodrigues, *Nat. Chem.*, 2019, **11**, 402.
15 K. E. D. Coan and B. K. Shoichet, *J. Am. Chem. Soc.*, 2008, **130**, 9606.
16 X. Qiu, Q. Kong, M. Zhou and D. Yang, *J. Phys. Chem. B*, 2010, **114**, 15857.
17 S. Gupta, R. Tyagi, V. S. Parmar, S. K. Sharma and R. Haag, *Polymer*, 2012, **53**, 3053.
18 J. d. F. Poloni, H. Chapola, B. C. Feltes and D. Bonatto, *Biol. Cell*, 2014, **106**, 167.
19 M. P. Espaillat, A. A. Shamseddine, M. M. Adada, Y. A. Hannun and L. M. Obeid, *Transl. Cancer Res.*, 2015, **4**, 484.
20 F. Darios, C. Wasser, A. Shakirzyanova, A. Giniatullin, K. Goodman, J. L. Munoz-Bravo, J. Raingo, J. Jorgačevski, M. Kreft, R. Zorec, J. M. Rosa, L. Gandia, L. M. Gutiérrez, T. Binz, R. Giniatullin, E. T. Kavalali and B. Davletov, *Neuron*, 2009, **62**, 683.
21 N. J. Haughey, V. V. R. Bandaru, M. Bai and M. P. Mattson, *Biochim. Biophys. Acta*, 2010, **1801**, 878.
22 X. He, Y. Huang, B. Li, C.-X. Gong and E. H. Schuchman, *Neurobiol. Aging*, 2010, **31**, 398.
23 A. Poujois, J.-C. Devedjian, C. Moreau, D. Devos, P. Chaine, F. Woimant and J. A. Duce, *Curr. Treat. Options Neurol.*, 2016, **18**, 46.
24 M. G. Savelieff, G. Nam, J. Kang, H. J. Lee, M. Lee and M. H. Lim, *Chem. Rev.*, 2019, **119**, 1221.
25 K. P. Kepp, *Chem. Rev.*, 2012, **112**, 5193.
26 I. W. Hamley, *Chem. Rev.*, 2012, **112**, 5147.
27 B. R. Roberts, T. M. Ryan, A. I. Bush, C. L. Masters and J. A. Duce, *J. Neurochem.*, 2012, **120**, 149.
28 K. Acevedo, S. Masaldan, C. M. Opazo and A. I. Bush, *J. Biol. Inorg. Chem.*, 2019, **24**, 1141.
29 A. S. DeToma, S. Salamekh, A. Ramamoorthy and M. H. Lim, *Chem. Soc. Rev.*, 2012, **41**, 608.
30 B. Alies, A. Conte-Daban, S. Sayen, F. Collin, I. Kieffer, E. Guillon, P. Faller and C. Hureau, *Inorg. Chem.*, 2016, **55**, 10499.
31 P. Dorlet, S. Gambarelli, P. Faller and C. Hureau, *Angew. Chem., Int. Ed.*, 2009, **48**, 9273.

32 M. G. Savelieff, S. Lee, Y. Liu and M. H. Lim, *ACS Chem. Biol.*, 2013, **8**, 856.
33 P. Faller, C. Hureau and O. Berthoumieu, *Inorg. Chem.*, 2013, **52**, 12193.
34 P. Faller, C. Hureau and G. L. Penna, *Acc. Chem. Res.*, 2014, **47**, 2252.
35 S. Vivekanandan, J. R. Brender, S. Y. Lee and A. Ramamoorthy, *Biochem. Biophys. Res. Commun.*, 2011, **411**, 312.
36 F. M. LaFerla, K. N. Green and S. Oddo, *Nat. Rev. Neurosci.*, 2007, **8**, 499.
37 T. Harayama and H. Riezman, *Nat. Rev. Mol. Cell Biol.*, 2018, **19**, 281.
38 K. L. Hentchel and J. C. Escalante-Semerena, *Microbiol. Mol. Biol. Rev.*, 2015, **79**, 321.
39 M. Taguchi, K. Sugimoto, K.-i. Goda, T. Akama, K. Yamamoto, T. Suzuki, Y. Tomishima, M. Nishiguchi, K. Arai, K. Takahashi and T. Kobori, *Bioorg. Med. Chem. Lett.*, 2003, **13**, 1963.
40 P. Wisse, H. Gold, M. Mirzaian, M. J. Ferraz, G. Lutteke, R. J. B. H. N. v. d. Berg, H. v. d. Elst, J. Lugtenburg, G. A. v. d. Marel, J. M. F. G. Aerts, J. D. C. Codée and H. S. Overkleeft, *Eur. J. Org. Chem.*, 2015, 2661.
41 I. Ojima and E. S. Vidal, *J. Org. Chem.*, 1998, **63**, 7999.
42 P. Sanllehí, J.-L. Abad, J. Bujons, J. Casas and A. Delgado, *Eur. J. Med. Chem.*, 2016, **123**, 905.
43 X. Cong, F. Hu, K.-G. Liu, Q.-J. Liao and Z.-J. Yao, *J. Org. Chem.*, 2005, **70**, 4514.
44 P. Muller, *Pure Appl. Chem.*, 1994, **66**, 1077.
45 W. Al-Soufi, L. Piñeiro and M. Novo, *J. Colloid Interface Sci.*, 2012, **370**, 102.
46 E. Opatowski, M. M. Kozlov, I. Pinchuk and D. Lichtenberg, *J. Colloid Interface Sci.*, 2002, **246**, 380.
47 K. J. Korshavn, A. Bhunia, M. H. Lim and A. Ramamoorthy, *Chem. Commun.*, 2016, **52**, 882.
48 T. H. Kee, P. Vit and A. J. Melendez, *Clin. Exp. Pharmacol. Physiol.*, 2005, **32**, 153.
49 R. G. Pearson, *J. Am. Chem. Soc.*, 1963, **85**, 3533.
50 R. D. Hancock and M. P. Ngwenya, *J. Chem. Soc., Dalton Trans.*, 1987, 2911.
51 C. S. Atwood, R. D. Moir, X. Huang, R. C. Scarpa, N. M. E. Bacarra, D. M. Romano, M. A. Hartshorn, R. E. Tanzi and A. I. Bush, *J. Biol. Chem.*, 1998, **273**, 12817.
52 W. R. Harris, C. J. Carrano, S. R. Cooper, S. R. Sofen, A. E. Avdeef, J. V. McArdle and K. N. Raymond, *J. Am. Chem. Soc.*, 1979, **101**, 6097.
53 T. Storr, M. Merkel, G. X. Song-Zhao, L. E. Scott, D. E. Green, M. L. Bowen, K. H. Thompson, B. O. Patrick, H. J. Schugar and C. Orvig, *J. Am. Chem. Soc.*, 2007, **129**, 7453.
54 H. Irving and R. J. P. Williams, *J. Chem. Soc.*, 1953, 3192.
55 G. Micera, S. Deiana, A. Dessi, P. Decock, B. Dubois and H. Kozlowski, *Inorg. Chim. Acta*, 1985, **107**, 45.
56 H. Kozlowski, P. Decock, I. Olivier, G. Micera, A. Pusino and L. D. Pettit, *Carbohydr. Res.*, 1990, **197**, 109.
57 J.-C. Zheng, R. J. Rousseau and S. Wang, *Inorg. Chem.*, 1992, **31**, 106.
58 J. Danielsson, R. Pierattelli, L. Banci and A. Gräslund, *FEBS J.*, 2007, **274**, 46.
59 S.-J. Hyung, A. S. DeToma, J. R. Brender, S. Lee, S. Vivekanandan, A. Kochi, J.-S. Choi, A. Ramamoorthy, B. T. Ruotolo and M. H. Lim, *Proc. Natl. Acad. Sci. U. S. A.*, 2013, **110**, 3743.
60 J. J. Braymer, J.-S. Choi, A. S. DeToma, C. Wang, K. Nam, J. W. Kampf, A. Ramamoorthy and M. H. Lim, *Inorg. Chem.*, 2011, **50**, 10724.
61 J. W. Karr, H. Akintoye, L. J. Kaupp and V. A. Szalai, *Biochemistry*, 2005, **44**, 5478.
62 S. C. Drew, S. L. Leong, C. L. L. Pham, D. J. Tew, C. L. Masters, L. A. Miles, R. Cappai and K. J. Barnham, *J. Am. Chem. Soc.*, 2008, **130**, 7766.
63 S. C. Drew, *Appl. Magn. Reson.*, 2015, **46**, 1041.
64 G. J. Troup, L. Navarini, F. S. Liverani and S. C. Drew, *PLoS One*, 2015, **10**, e0122834.
65 W. Bal, H. Kozlowski, M. Lisowski, L. Pettit, R. Robbins and A. Safavi, *J. Inorg. Biochem.*, 1994, **55**, 41.
66 A. Hecel, C. Migliorini, D. Valensin, M. Luczkowski and H. Kozlowski, *Dalton Trans.*, 2015, **44**, 13125.
67 A. Hecel, S. Draghi, D. Valensin and H. Kozlowski, *Dalton Trans.*, 2017, **46**, 7758.
68 G. Nam, M. Hong, J. Lee, H. J. Lee, Y. Ji, J. Kang, M.-H. Baik and M. H. Lim, *Chem. Sci.*, 2020, **11**, 10243.
69 S. A. Kotler, P. Walsh, J. R. Brender and A. Ramamoorthy, *Chem. Soc. Rev.*, 2014, **43**, 6692.
70 W. Zheng, J. Kollmeyer, H. Symolon, A. Momin, E. Munter, E. Wang, S. Kelly, J. C. Allegood, Y. Liu, Q. Peng, H. Ramaraju, M. C. Sullards, M. Cabot and A. H. Merrill, Jr, *Biochim. Biophys. Acta*, 2006, **1758**, 1864.
71 S. M. Crivelli, C. Giovagnoni, L. Visseren, A.-L. Scheithauer, N. d. Wit, S. d. Hoedt, M. Losen, M. T. Mulder, J. Walter, H. E. d. Vries, E. Bieberich and P. Martinez-Martinez, *Adv. Drug Delivery Rev.*, 2020, **159**, 214.
72 D. Piomelli, G. Astarita and R. Rapaka, *Nat. Rev. Neurosci.*, 2007, **8**, 743.
73 V. Rangachari, D. N. Dean, P. Rana, A. Vaidya and P. Ghosh, *Biochim. Biophys. Acta*, 2018, **1860**, 1652.
74 K. Yang and X. Han, *Trends Biochem. Sci.*, 2016, **41**, 954.
75 Z. Niu, Z. Zhang, W. Zhao and J. Yang, *Biochim. Biophys. Acta*, 2018, **1860**, 1663.
76 K. J. Korshavn, C. Satriano, Y. Lin, R. Zhang, M. Dulchavsky, A. Bhunia, M. I. Ivanova, Y.-H. Lee, C. L. Rosa, M. H. Lim and A. Ramamoorthy, *J. Biol. Chem.*, 2017, **292**, 4638.
77 M. Kinoshita, E. Kakimoto, M. S. Terakawa, Y. Lin, T. Ikenoue, M. So, T. Sugiki, A. Ramamoorthy, Y. Goto and Y.-H. Lee, *Phys. Chem. Chem. Phys.*, 2017, **19**, 16257.
78 M. S. Terakawa, Y. Lin, M. Kinoshita, S. Kanemura, D. Itoh, T. Sugiki, M. Okumura, A. Ramamoorthy and Y.-H. Lee, *Biochim. Biophys. Acta*, 2018, **1860**, 1741.